Heliyon 10 (2024) e36366

Contents lists available at ScienceDirect

Heliyon

journal homepage: www.cell.com/heliyon

Research article

Photosystem modulation and extracellular silicification in green microalgae: Key strategies for lead tolerance and removal

Fiaz Ahmad [a,*], Michael Manefield [b]

[a] Key Laboratory for Space Bioscience & Biotechnology, School of Life Sciences, Northwestern Polytechnical University, Xi'an, 710072, People's Republic of China

[b] School of Civil and Environmental Engineering, University of New South Wales (UNSW), Sydney, 2052, New South Wales, Australia

ARTICLE INFO

Keywords:
Green microalgae
Novel isolate
RSM
Pb^{+2} removal
Silicification
Survival mechanisms
Cell physiology
Quantum yield
Non-photochemical quenching

ABSTRACT

The escalating contamination caused by lead ions (Pb^{2+}) and its harmful effects on all life forms has raised global concerns. Certain microalgae thrive in metal mining sites characterized by low pH and high concentrations of Pb^{2+}, which are usually prohibitive for many microorganisms. Little is known about the mechanisms underlying the adaptation of such microalgae to these hostile conditions. In this study, we elucidated the adaptive strategies of the green microalga *Micractinium belenophorum* strain AUMW, isolated from a lead mining site, and its application for the removal of Pb^{+2}. Results revealed that strain AUMW can efficiently tolerate up to 200 ppm of Pb^{+2} in an F/2 medium. Further experimental variables were optimized through response surface methodology (RSM), and 99.6 % removal of Pb^{2+} was achieved. Novel adaptive responses of strain AUMW to high levels of Pb^{2+} include: (i) activation of metal-protective response by modulation of quantum yield (F_v/F_m) and non-photochemical quenching (NPQ) of photosystem II; (ii) extracellular silicification encapsulated cells of strain AUMW and altered cell morphology from oval to hexagonal; (iii) silicification prevented intracellular translocation of Pb^{+2}; (iv) silicification boosted adsorption of Pb^{+2}, thus enhanced its removal. This study offers new insights into the protective role of silicification in green microalgae and its potential for the removal of metals from metal-polluted sites, waste from energy storage battery industries, and spent batteries. It also provides a solid base to explore the genetic and metabolic pathways involved in the adaptation of strain AUMW to elevated levels of Pb^{+2}.

1. Introduction

Heavy metals (HMs) constitute a major component of inorganic pollutants, presenting serious environmental concerns due to their high toxicity, non-biodegradability, rapid accumulation in the food chain, and continuously increasing concentrations [1,2]. Being non-biodegradable and persistent direct exposure to lead ions (Pb^{+2}) can cause irreversible damage to human health [3]. With ever-increasing industrialization, the demand for lead continues to rise, leading to an inevitable release of lead ions Pb^{+2} into the environment through excavation and mining, e-waste dismantling, and chemical manufacturing [4–6]. This persistent use of Pb^{+2} and the resulting pervasive pollution have provoked significant interest among researchers in developing eco-friendly, sustainable biogenic strategies for the removal of Pb^{+2} effectively [7,8], to hinder indirect or direct adverse effects on human health and eco-system.

* Corresponding author.
E-mail address: fiaz.a@mail.nwpu.edu.cn (F. Ahmad).

https://doi.org/10.1016/j.heliyon.2024.e36366
Received 4 June 2024; Received in revised form 13 August 2024; Accepted 14 August 2024
Available online 15 August 2024
2405-8440/© 2024 The Authors. Published by Elsevier Ltd. This is an open access article under the CC BY-NC-ND license (http://creativecommons.org/licenses/by-nc-nd/4.0/).

To date, various physicochemical methods, such as the use of biopolymers, dried plant parts, zeolites, chemical precipitation, ion exchange, coagulation, and flocculation, have been implemented to remove HMs from polluted soil and water [9–11]. However, complex preparation processes, the high cost of adsorbents, and their non-ecofriendly nature may limit their application in real-world environments. Consequently, bioremediation approaches using microorganisms to remove Pb^{+2} have gained attention within the scientific community [12–14]. Various microalgal strains isolated from metal-polluted sites have demonstrated higher potential for metal removal and detoxification through mechanisms such as sequestration, enzymatic detoxification, and active transport of metals [15]. Such microalgal strains are ideal candidates for bioremediation of metal-polluted sites. Documented research revealed that the microbial capability for the removal of metals is largely dependent on operational conditions [16,17]. Therefore, we used response surface methodology (RSM), an orthogonal statistical design for the optimization of different operational conditions to assist microalgae for enhanced removal of Pb^{+2}.

Recently, a study reported 79 % removal of Pb^{+2} from diluted industrial wastewater using consortia of the alga *Chlorella vulgaris* and the bacterium *Enterobacter* sp. MN17 [18]. However, the efficiency of this consortium in undiluted conditions and its survival under natural conditions remains uncertain. A recent review investigating Pb^{+2} and Cd^{+2} removal highlighted that thermodynamic equilibrium between microalgae and HMs is influenced by the type of microalgal species and their affinity towards HMs, indicating different species exhibit varying rates of metal removal [19]. While, fine powdered biomass of *Chlorella sorokiniana* has been reported to achieve 90 % Pb^{+2} removal via adsorption within the concentration range of 5–200 ppm [20].

Among different strategies for using microbes or microbial products for the removal of HMs, the use of microbial consortia has recently been considered highly efficient because they synergistically enhance metal removal [21]. For example, a designed consortium of three bacteria [(*Bacillus* sp., (NCBI Acc. No. MK999907), *Bacillus* sp. (NCBI Acc. No. MN005950), and *Micrococcus* sp. (NCBI Acc. No. MN005949)], two microalgae [*Scenedesmus acutus* (NCIM 5584) and *Chlorella pyrenoidosa* (NCIM 2738)], and their mixture in equal quantities were investigated for Pb^{+2} and Cd^{+2} removal from solutions containing individual metals and metal mixtures. The maximum Pb^{+2} removal by the bacterial and algal consortia alone was 60.29 % and 54.95 %, respectively, while the mixed bacterial-algal consortium achieved up to 98 % Pb^{+2} removal [22]. However, we hypothesize that microalgal strains proliferating at metal mining sites for prolonged periods may have evolved specific mechanisms to mitigate Pb^{+2} toxicity. If some strains are efficient enough, they may eliminate the need for establishing suitable microbial consortia and their cultivation conditions, ultimately saving time and resources.

Therefore, this study aimed to isolate a novel Pb^{+2}-tolerant microalga from a lead mining site and investigate its efficacy for: i) tolerance to Pb^{+2}, ii) use of RSM for determining optimized operational conditions for enhanced removal of Pb^{+2} from F/2 medium, iii) the effect of Pb^{+2} on the growth and physiology of strain AUMW, and iv) elucidating the mechanisms of strain AUMW's survival and Pb^{+2} removal at 100 ppm and 200 ppm initial concentrations of Pb^{+2}. The use of state-of-the-art techniques, including sequencing, PAM, ICP-MS, FE-STEM, elemental mapping, FTIR, EDS, and electron diffractometry, revealed the identity of the isolate, the reciprocity between F_v/F_m and NPQ of photosystem II, quantitative analysis of lead, and the localization and characterization of lead and silica on algal cells to achieve the goals of this study. To our knowledge, mechanisms of green microalgae-mediated Pb^{+2} removal and its survival discovered in this study have never been reported elsewhere.

2. Materials and methods

2.1. Reagents and culture media

Analytical grade lead nitrate $Pb(N_2O_6)$ with a purity of ≥99 % was acquired from Sinopharm Chemical Reagent Co., Ltd., Shaanxi, China. Primers used in this study were sourced from Sangon Biotech Co., Ltd., Shanghai, China. Deionized distilled water was obtained from Milli-Q system (MilliporeSigma, Bedford, MA, USA). A modified Gaillard's F/2 marine enrichment culture medium was prepared by dissolving 35 g of commercial-grade sea salt in 1 L of distilled deionized water (ddH_2O), followed by vacuum filtration through a 0.45 μm pore-size filter paper. Tris(hydroxymethyl)aminomethane (Tris) was added to this solution to achieve a final concentration of 1.21 g/L. Tris was completely dissolved before adjusting the pH of the solution to 7.5 ± 0.1 by the gradual addition of concentrated hydrochloric acid (HCl). The solution was then sterilized by autoclaving at 120 °C for 20 min.

Subsequently, 5 mL/L of a 20 % w/v sodium nitrate ($NaNO_3$) solution, 5 mL of a 1.3 % w/v sodium phosphate monobasic (NaH_2PO_4. H_2O) solution, and 1 mL/L of F/2 trance metal solution were added aseptically. For solid media preparations, 8 % (w/v) agar-agar powder was incorporated into the liquid F/2 medium to formulate F/2-agar plates. All components for the F/2 medium were procured from Sangon Biotech Co., Ltd., Shanghai, China, with a purity of ≥99 %.

2.2. Isolation of novel microalgal strains

To isolate potential heavy metal-tolerant microalgal strains, soil samples were collected from a lead (Pb) mining site. Homogenized samples comprising 10 g of soil were dispensed into 100 mL of F/2 medium spiked with 25 ppm of lead ions (Pb^{+2}) and poured into 250 mL Erlenmeyer flasks. The cultures were incubated at 26 °C, following an 8-h dark and 16-h light cycle with a light intensity of 100 μmol photons m^{-2} s^{-1}. After two weeks of incubation, a 5 mL aliquot from the homogenized culture was transferred to fresh F/2 medium containing Pb^{+2}, and the incubation cycle was repeated for an additional 15 days. This step was performed three times to enrich and support the growth of the surviving microalgal strains. Successive tenfold serial dilutions from the final culture were plated on sterile F/2-agar plates supplemented with 25 ppm of Pb^{+2}, in triplicate. The plates were incubated under the previously described conditions until distinct, green colonies were observed. The most rapidly growing microalgae were selected and purified among the

emergent isolates for subsequent studies. In similar experimental setups, the only variation was the substitution of the F/2 cultivation medium with the BG-11 medium (freshwater microalgae cultivation medium). However, the microalgal strains failed to survive in the BG-11 medium. Therefore, for this study, the F/2 medium was utilized for microalgal cultivation.

2.3. Identification of the algal isolate

For genetic identification, a freshly grown single colony of the novel microalga was subjected to colony polymerase chain reaction (PCR) and sequencing of the 18S rRNA gene amplified by using a primer set (18S–F1 5'-GAGACGGCTACCACATCCAAGG-3', and 18S-R1 5'-ACAAAGGGCAGGGACGTAATCA-3'). Briefly, a microalgal colony was suspended aseptically in 1 mL of F/2 medium, heated at 99 °C for 35–45 s, and then 1 μL of the cooled suspension was used as a template for the PCR. The resulting 18S rRNA gene amplicon was sequenced by Sangon Biotech Co., Ltd., Shanghai, China. The obtained sequence was compared against reference sequences of type strains using the Basic Local Alignment Search Tool (BLAST) at NCBI and subsequently submitted to GenBank. A phylogenetic tree was constructed using MEGA-X software to analyse the relationship between our isolate and reference microalgae sequences.

2.4. Screening of microalga for survival against different concentrations of Pb^{+2}

The Pb^{+2} tolerance of strain AUMW was assessed by cultivating it in F/2 medium supplemented with varying concentrations of Pb^{+2}. Fresh seed culture of strain AUMW was incubated in cylindrical photobioreactors (PBR) at 25 °C under a light/dark regime of 16/8 h at 100 μmol photons m^{-2} s^{-1}, with an airflow of 1.5 m^3 min^{-1} filtered through a 0.22 μm filter. At the exponential growth phase, cultures were harvested and prepared for subsequent experiments examining the effects of different Pb^{+2} concentrations on algal growth. Algal cultures harvested from PBR were centrifuged at 5000 rpm for 10 min. The supernatant was discarded, and the pellet was thrice rinsed with sterile distilled water (dH_2O), then resuspended in fresh dH_2O to serve as stock seed culture. All experimental controls and treatments had a uniform initial optical density of 1.0 at 750 nm (OD_{750}). The growth behavior of strain AUMW was observed in triplicate within 50 mL Erlenmeyer flasks, each containing 25 mL of F/2 medium enriched with a gradient of Pb^{+2} concentrations (0, 20, 40, 80, 120, and 160 ppm). Sampling was performed at 2, 4, 6, 8, and 10 days post-incubation to measure the OD_{750}, cell number, and cell size.

2.5. Operational parameter optimization for Pb^{+2} removal

Our previous work showed significant enhancement in silver removal by axenic bacteria and bispyribac sodium degradation by axenic as well as co-cultured bacteria when experimental conditions were optimized using an orthogonal statistical design [16,23]. In this study, we identified that factors like Pb^{+2} concentration, pH, and temperature influenced the growth of strain AUMW. These factors, along with cultivation time, were optimized using the central composite design (CCD) of response surface methodology (RSM) of Design-Expert® 12, covering 30 runs (Table S1), to improve Pb^{+2} removal capacity of strain AUMW from F/2 medium. Each experiment was biologically replicated three times to ensure reliability. Symbols and levels of these factors are cataloged in Table 1. Outcome measures of Pb^{+2} removal percentages were taken at several time points e.g. 1, 2, 4, 6, 24, 48, and 72 post-inoculation, and residual concentrations of Pb^{+2} were quantified by Inductively Coupled Plasma Mass Spectrometry (ICP-MS). The process was captured by quadratic polynomial equations (Eq. I & II) [16,24], analysed for interactions and coefficients, and visualized using three-dimensional (3-D) surface and two-dimensional (2-D) contour plots.

$$WY = z0 + z1A + z2B + z3C + z4D + z12\,AB + z13AC + z23AD + z24BC + z25BD + z26CD + z11A2 + z22B2 + z33C2 + z44D2 \quad (1)$$

In Equation I, Y represents the predicted outcome, while z0 indicates the fitted response at the centre point of the CCD design; z1, z2, z3, and z4 denote the linear coefficients; z12, z13, z23, z24, z25, and z26 represent the interaction coefficients; z11, z22, z33, and z44 signify the quadratic coefficients for Pb^{+2} removal. The model was validated by its correlation coefficient (R^2) and an F-test, with further confirmation by comparing predicted and actual values of Pb^{+2} removal. While analysis of variance (ANOVA) elucidated significant and non-significant differences among different treatments.

Table 1
Symbols and levels of independent experimental variables investigated for % removal of Pb^{+2} by strain AUMW.

Variables	Units	Symbols	Coded levels (Range)		
			Low (−1)	Mean (0)	High (+1)
Time	h	A	1	36	72
Temperature	°C	B	20	35	50
pH	-log[H+]	C	3	6.5	10
Initial concentration of Pb^{+2}	ppm	D	50	100	150

2.6. The experimental setup for algal strain AUMW mediated Pb^{+2} removal

Triplicate batch cultures investigated the Pb^{+2} bioaccumulation efficacy of strain AUMW in 25 mL F/2 media within 50 mL Erlenmeyer flasks, fortified with either 100 ppm or 200 ppm Pb^{+2}. The study design included three controls and two treatments: Control groups consisted of (1) a culture of AUMW in F/2 medium serving as a control for growth metrics, referred to as X1; (2) an F/2 medium supplemented with 100 ppm of Pb^{+2} but not inoculated with AUMW, designated as W2; and (3) an F/2 medium supplemented with 200 ppm of Pb^{+2} but not inoculated with AUMW, named W3, to evaluate the respective residual lead concentrations in samples after treatment applied. The treatment groups comprised F/2 medium augmented with (1) 100 ppm of Pb^{+2} (X2) and (2) 200 ppm of Pb^{+2} (X3), both inoculated with strain AUMW. Axenic strain AUMW seed culture was inoculated to achieve an initial OD_{750} of 1.0 across all experimental setups. The cultures were incubated on a rotary shaker at 26 °C and 200 rpm, under a day cycle of 8 h dark and 16 h light at 100 μmol photons m^{-2} s^{-1}. Periodic sampling was performed at 1, 2, 4, 6, 24, 48, and 72 h post-inoculation, where OD_{750} measurements were used to quantify the growth of AUMW. Following each time point, AUMW's cell pellets and supernatants were harvested for subsequent microscopic analysis and quantification of Pb^{+2} residual concentrations via ICP-MS, respectively.

2.7. PAM fluorometric analysis of algal strain AUMW

The real-time effects of Pb^{+2} stress on strain AUMW were monitored using a Chlorophyll Fluorometer AquaPen AP 110-C (Heinz Walz GmbH, Effeltrich, Germany). This device includes a PIN photodiode detector with bandpass filters operating at wavelengths ranging from 665 to 750 nm. These filters selectively filter out the red light emanating from LEDs or the water surface. A 4 mL aliquot from each experimental and control sample was taken for fluorescence assessments and acclimated in darkness for 15–30 min before data collection. We measured non-photochemical quenching (NPQ) and the maximum quantum yield of photosystem II (F_v/F_m) of the microalgae.

2.8. Elucidation of Pb^{+2} removal strategy of algal strain AUMW

The process underlying Pb^{+2} sequestration by strain AUMW and the role of mineral adsorption on algal cells in Pb^{+2} detoxification and enhancement of algal resilience were investigated utilizing a high-resolution Field Emission Scanning Transmission Electron Microscope (FE-STEM; Thermo Scientific Talos™ F200X G2). The FE-STEM system was equipped with energy-dispersive X-ray spectroscopy (EDS) detectors, a high-sensitivity complementary metal-oxide-semiconductor (CMOS) camera, and a sophisticated Lorentzian lens for capturing detailed dark-field and bright-field images. To prepare for imaging, cells from treatments X2 and X3 were sequentially dehydrated in an ethanol gradient of 30 %, 50 %, 70 %, 90 %, and 100 %, each step lasting 15–20 min. Subsequently, 5–10 μL of the cell suspension was applied to a carbon-coated grid and air-dried at room temperature. These samples were then analysed under the FE-STEM to identify the localization of mineralized Pb^{+2} and elements of Si, carbon (c), and oxygen (O_2) to differentiate cellular entities and adsorbed minerals. The visualization of cellular features was improved using dark-field and bright-field imaging methods. Findings of elemental mapping (EM) and structural details were further clarified using energy dispersive spectroscopy (EDS) and electron diffraction patterns.

2.9. FTIR analysis

To determine the origin of Si in the cultivation medium, we analysed the chemical composition of key ingredients such as sea salt and $Pb(N_2O_6)$ of cultivation medium F/2. Additionally, we utilized sodium metasilicate ($Na_2SiO_3.9H_2O$) as a control for Si content. This analysis was conducted using Fourier transform infrared (FTIR) spectroscopy (BRUKER Tensor 27 IR, Germany). Samples were prepared following FTIR manufacturer's instructions. Briefly, about 1–2 mg of $Pb(N_2O_6)$, seal salt, and $Na_2SiO_3.9H_2O$ were mixed with 300–400 mg of potassium bromide, and spectra of each sample were recorded with a scanning range of 400–4000 cm^{-1}. Band stretching of different functional groups, mainly focusing on Si bonds with other elements, was recorded to identify the major source of Si in the solution.

2.10. Data analysis

All experiments were performed in triplicate with biological replicates, and the data were presented as mean values ± standard deviation (±SD). Analysis of Variance (ANOVA) was performed on data for Pb^{2+} removal, OD750, cell number, and cell size using the SPSS software package. Values with $p < 0.05$ were considered significantly different.

3. Results and discussion

3.1. Identification and Pb^{+2} tolerance potential of algal strain AUMW

A Pb^{+2}-tolerant green microalgal strain AUMW was isolated, and achieved clonal purity. Sequencing of the 18S rRNA gene and subsequent alignment with the NCBI reference database revealed 99.5 % sequence similarity of strain AUMW with the genus *Micractinium*. Phylogenetic analysis placed the strain in a distinct clade adjacent to *Micractinium belenophorum* (Fig. S1). The gene sequence was submitted to NCBI-GenBank and obtained the accession number PP094557. The genus *Micractinum* has been reported for

its high cryptic diversity and distribution in diverse biotopes [25]. However, information on the distribution of specie *belenophorum* is elusive. The discovery of new microalgae is not only essential for sustainable recycling and environmental sustainability but also a potential source for sustainable production of value-added products for their production in diverse fields [26,27].

The response of strain-AUMW to various Pb^{+2} concentrations (20, 40, 80, 120, and 160 ppm) in F/2 medium was monitored. Growth rates, determined by OD_{750} readings over a 10-day cultivation period, revealed a Pb^{+2} dose-dependent inhibition of strain-AUMW's proliferation. Despite this inhibition, strain AUMW exhibited a continued increase in growth up to day 10 at all tested Pb^{+2} concentrations, indicating its ability to tolerate these levels of Pb^{+2} (Fig. 1a). These findings suggested that strain AUMW has evolved mechanisms to withstand high Pb^{+2} concentrations, likely due to its origin in soil and water from a lead mining site.

The tolerance of strain AUMW to a range of Pb^{+2} concentrations in connection to its reported ecological plasticity [25,28], suggested that strain AUMW could be a prime candidate for bioremediation of metal-contaminated soil, water, and lead battery industrial waste. To the best of the author's knowledge, *Micractinium belenophorum* has not been previously reported for the removal of metals. However, the genus *Micractinium* has been documented for wastewater treatment and nutrient removal [29,30].

3.2. RSM-mediated optimization of Pb^{+2} removal by strain AUMW

A regression analysis was performed on the data from RSM-based experiments on Pb^{+2} removal by strain AUMW, yielding a polynomial quadratic equation (Eq. II) that expresses the percentage of Pb^{+2} removal, as reported in our previous work [16,23,31].

$$Y = 52.28 + 3.29A - 4.20B + 19.59C + 8.94D - 0.86AB - 0.62AC - 2.39AD + 5.23BC - 0.95BD - 6.17CD - 2.48A^2 + 1.47B^2 + 1.11C^2 + 4.14D^2 \quad (2)$$

In this equation, 'Y' predicts the efficacy of Pb^{+2} removal as defined by the CCD model, with A, B, C, and D representing time, temperature, pH, and initial Pb^{+2} concentration, respectively. The positive and negative signs indicate the synergistic and adverse effects of these parameters on Pb^{+2} removal potential of strain AUMW. The actual experimental values and the predicted ones from the CCD model of RSM are listed in (Table 2). Experimental data closely matched the model's predictions, as shown by the parity plot (Fig. 1b), where points clustered near the diagonal line indicate an excellent model fit.

The significance of experimental variables within Eq. II was quantified by their p-values and the regression coefficient (R^2). An R^2 value of 0.97 confirms that the variation in the percent removal of Pb^{+2} is largely influenced by the experimental variables. Individual and interactive effects of the experimental variables with P-values <0.05 were considered significant, while P-values <0.01 were highly significant. Analysis of variance (ANOVA) results validated the accuracy of the CCD model, with a significant F-test value of 36.21 and a highly significant p-value of 0.0001. Additionally, the significant lack of fit of the CCD model, with an F-value of 3.33 and a P-value of 0.0482 (Table 3), confirmed that the model is acceptable.

Three-dimensional (3-D) surface (Fig. 2a) and two-dimensional (2-D) contour (Fig. 2b) plots describing the interactive and individual impact of experimental variables on the response of the CCD model that is % removal of Pb^{+2}. Results revealed that temperature and time had a non-significant influence on Pb^{+2} removal potential of strain AUMW. However, at 40–50 °C slight increase in Pb^{+2} removal was recorded after 48 h of incubation (Fig. 2a1), this increase could be attributed to the partial disruption of the cell wall of strain AUMW, resulting in the release of intracellular macromolecules scavenging Pb^{+2} from the aqueous solution. This outcome is supported by recent literature showing temperature and pH-dependent cell wall disruption for lipid extraction. A 96.4 % lipid yield was achieved at 45 °C and pH 4.4 in 190 min, while 70 % was extracted at 36 °C and pH 5 in 90 min in association with chemical and enzyme treatments, respectively [32]. Recently we reported metal ions to mineralize into metallic nanoparticles by interacting with bacterial extracellular proteins [16,33], and elsewhere metallic nanoparticles are reported for their enzymatic activities [34], as well

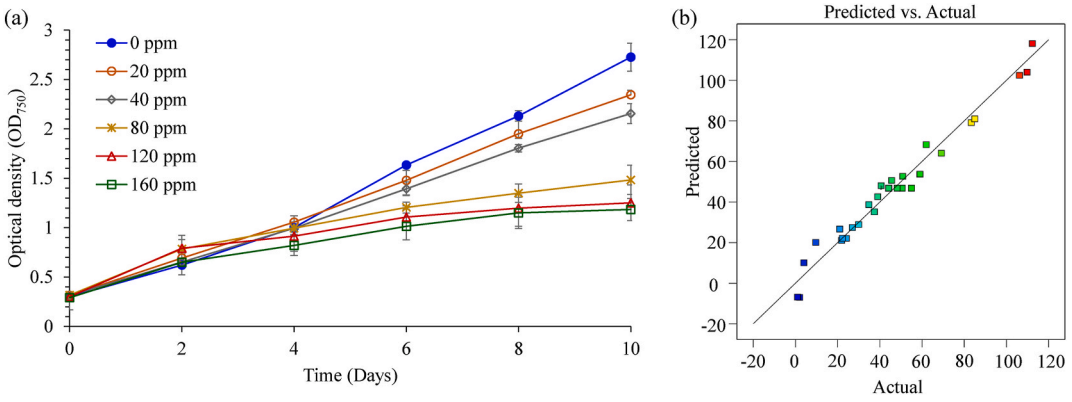

Fig. 1. Growth response of strain AUMW to varying concentrations of Pb+2 and optimization using response surface methodology (RSM). **(a)** Demonstrates a reduction in AUMW's growth correlating with exposure to incrementally higher levels of Pb+2, **(b)** Parity plot displaying an excellent model fit, evidenced by the close alignment of experimental data with the model's predicted values.

Table 2
The CCD matrix shows actual and predicted values of percent removal of Pb^{+2} by strain AUMW.

Order No.	Run No.	Variables in un-coded levels				Response (%Pb removal)	
		A	B	C	D	Actual	Predicted
5	1	3	20	10	50	30.000	28.900
2	2	9	20	3	50	27.000	27.460
15	3	3	50	10	150	109.800	104.017
8	4	9	50	10	50	22.300	22.130
30	5	6	35	6.5	100	44.200	46.840
6	6	9	20	10	50	1.000	0.831
25	7	6	35	6.5	100	44.200	46.842
22	8	6	35	13	100	21.000	26.686
20	9	6	65	6.5	100	62.000	68.269
7	10	3	50	10	50	21.870	21.123
12	11	9	50	3	150	83.340	79.122
16	12	9	50	10	150	106.200	102.414
3	13	3	50	3	50	2.000	1.973
13	14	3	20	10	150	85.000	80.999
23	15	6	35	6.5	0	4.000	10.078
14	16	9	20	10	150	39.000	42.656
11	17	3	50	3	150	50.880	52.699
18	18	12	35	6.5	100	34.790	38.704
28	19	6	35	6.5	100	50.600	46.840
21	20	6	35	1	100	9.660	20.067
9	21	3	20	3	150	69.200	64.052
26	22	6	35	6.5	100	55.000	46.840
24	23	6	35	6.5	200	112.300	118.141
29	24	6	35	6.5	100	48.200	46.840
1	25	3	20	3	50	37.400	35.174
10	26	9	20	3	150	59.00	53.734
27	27	6	35	6.5	100	44.200	46.840
19	28	6	5	6.5	100	45.600	50.659
17	29	0	35	6.5	100	40.600	48.014
4	30	9	50	3	50	24.070	22.059

Table 3
ANOVA for the response as % removal of Pb^{+2} by strain AUMW.

Source	Sum of Squares	df	F-value	*p*-value
	% removal of Pb^{+2}		% removal of Pb^{+2}	% removal of Pb^{+2}
Model	25543.25	14	36.21	0.0001[b]
A	130.01	1	2.58	0.129
B	465.17	1	9.23	0.008[a]
C	391.31	1	7.77	0.013[a]
D	17551.81	1	348.37	8.565
AB	1349.834	1	26.79	0.0001[b]
AC	785.40	1	15.58	0.0012[a]
AD	6.81	1	0.13	0.7182
BC	1181.30	1	23.44	0.0002[b]
BD	948.33	1	18.82	0.0005[b]
CD	539.17	1	10.70	0.0051[a]
A^2	21.10	1	0.41	0.5273
B^2	277.42	1	5.50	0.0330[a]
C^2	1155.38	1	22.93	0.0002[b]
D^2	447.52	1	8.88	0.0093[a]
Residual	755.73	15		
Lack of Fit	657.04	10	3.33	0.0482[a]

[a] = Significant.
[b] = Highly Significant: Values less than 0.0500 indicate the model terms are significant.

as causing oxidative damage to microalgal cell walls by denaturing lipids, proteins, and thiol peptides [35]. Suggesting that during Pb^{+2} removal by adsorption, mineralized nano-micro-sized particles of lead might be acting as nanozyme resulting in partial disruption of the cell wall of strain AUMW. Previous literature describes the varying trajectory of temperature effects on the removal of different metals by various microalgae, including adsorption [36], and biosorption [37,38].

A significant interactive effect was observed between pH and time, with pH levels of 7–9.6 enhancing Pb^{+2} removal (Fig. 2a2). This finding aligns with previous research indicating increased metal sequestration at elevated levels of pH such as a pH of 9.5 due to the availability of macromolecular functional groups to bind with metal cations [39,40]. A significant interaction between pH and

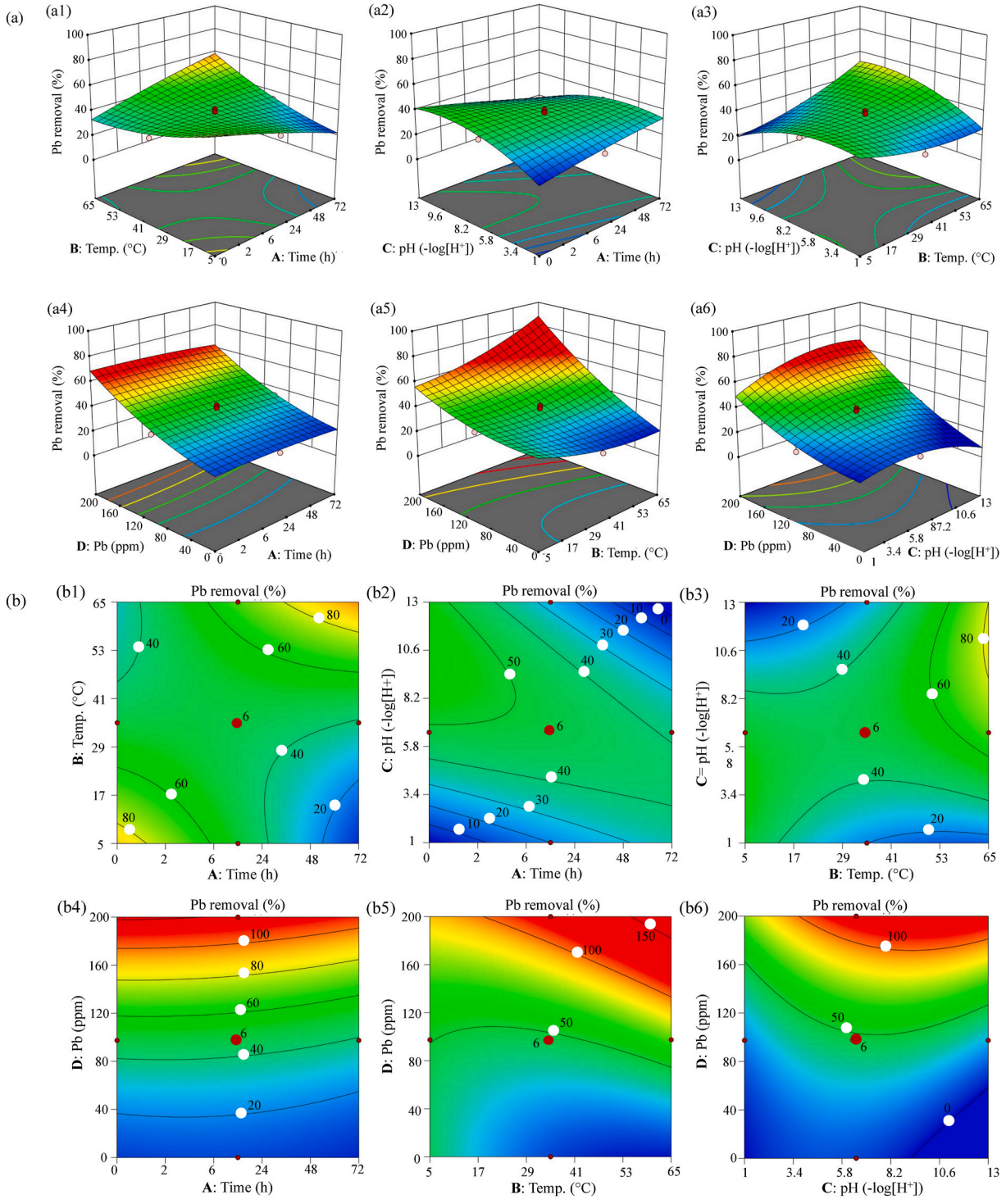

Fig. 2. 3-D and 2-D response surface methodology (RSM) plots for Pb+2 removal by strain AUMW. **(a)** 3-D surface and **(b)** 2-D contour plots illustrating the interaction and individual effects of experimental variables on the percent removal of Pb+2 by strain AUMW. **(a1, b1)** Represent the interaction and individual effects of incubation temperature and time, respectively, **(a2, b2)** depict the interaction and individual effects of pH and time, **(a3, b3)** show interaction and individual impacts of pH and temperature, **(a4, b4)** illustrate the interaction and individual influences of Pb+2 concentration and time, **(a5, b5)** present the interaction and individual effects of Pb+2 concentration and temperature, **(a6, b6)** demonstrate the interaction and individual effects of Pb+2 concentration and pH on the Pb+2 removal efficiency by strain AUMW.

temperature also emerged, identifying these factors as pivotal in optimizing removal efficiency; increased pH and temperature improved Pb^{+2} removal (Fig. 2a3). The surface plots showing interactions between initial Pb^{+2} concentrations with time (Fig. 2a4), temperature (Fig. 2a5), and pH (Fig. 2a6) indicated a continuous increase in Pb^{+2} removal with an increase in initial concentration of Pb^{+2}, whereas, time showed non-significant, temperature slightly significant, and pH showed highly significant effect on Pb^{+2} removal efficiency of strain AUMW, respectively. Previously documented reports suggest that metal removal increases with the escalated initial metal concentration up to saturation levels, after which the metal removal rate commences its downward trajectory [41].

The elliptical 2-D contour plots verified the significant effect of temperature-pH (Fig. 2b3) and initial Pb^{+2} concentration-pH interactions (Fig. 2b) on the efficiency of Pb^{+2} removal by strain AUMW. Optimal conditions yielded close to 90–92 % agreement between predicted and actual Pb^{+2} removal (Table 2).

3.3. *Pb^{+2} removal proficiency and survival adaptation in algal strain AUMW*

Under RSM-mediated optimized conditions, the Pb^{+2} removal efficiency of strain AUMW was assessed by measuring its concentration in the cell-free supernatants from treatment groups X2 and X3, in comparison with controls W2 and W3 (for details of these codes, see Section 2.6), using ICP-MS (Fig. 3a). Within 1 h of strain AUMW inoculation, 70 % and 90 % of Pb^{+2} was removed from X2 and X3, respectively. Notably, these efficiencies progressively increased over time, peaking at 97 % for X2 and 99.6 % for X3 after 72 h of treatment. Comparable findings of augmented removal efficiency with prolonged incubation were observed in other studies focused on iron and manganese by *Desmodesmus* sp. and *Heterochlorella* sp., though they did not surpass a 90 % threshold [42]. A recent study reported 98.69 % removal of Pb^{+2} by green microalgae *Haematococcus pluvialis* in 2 h, with a significant reduction in algal growth at Pb^{+2} concentrations up to 200 ppm [43]. In contrast, our work highlights the effectiveness of strain AUMW, which achieved 96.5 % of Pb^{+2} removal in 2 h and reached to 99.6 % by 72 h, with continuously increasing growth at 100 and 200 ppm of Pb^{+2}. However, further investigation is needed to elucidate the genetic and metabolic pathways involved in strain AUMW's survival and Pb^{2+} removal at elevated levels.

A time-dependent modulation in cellular growth parameters, including OD_{750}, cell number, and cell size, was observed over a 72 h experiment. Results revealed maximum growth in terms of OD_{750} for strain AUMW in X2, followed by X3 and X1, clearly showed growth promoting role of Pb^{+2} (Fig. 3b). In contrast, the cell number and cell size of AUMW showed an inverse relationship: the pattern of cell numbers was X1 > X2 > X3, while cell sizes followed the sequence X3 > X2 > X1 (Fig. 3c and d). These findings suggest that AUMW cells in X3 were able to adsorb more Pb^{+2} on their surface and exhibited larger cell sizes compared to those in X2, depending on the availability of Pb^{+2} in the aqueous medium. In addition, the reduced number of cells in X3 could be due to higher toxic pressure on AUMW cells compared to those in X2. Strain AUMW exhibited novel response mechanisms to Pb^{2+} exposure, showing enhanced growth and increased cell numbers and sizes compared to several reports that show a reduction in microalgal growth as the concentration of heavy metals increases [35,39].

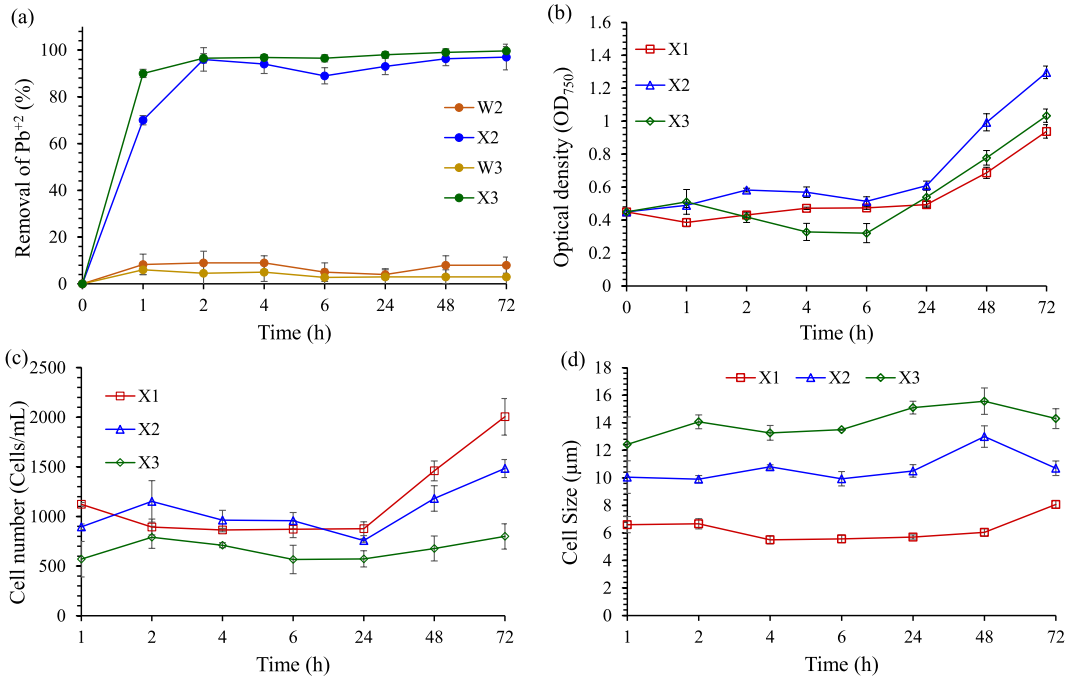

Fig. 3. Pb+2 removal efficiency of AUMW and impact of varying Pb+2 levels on its propagation. **(a)** Percentage of Pb+2 removal by AUMW from an F/2 solution enriched with 100 ppm and 200 ppm concentrations of Pb+2, along with the effects of these concentrations on **(b)** optical density at 750 nm (OD750), **(c)** cell count, and **(d)** cell size of AUMW.

3.4. Elucidating mechanism of the Pb^{+2} stress mitigation adapted by strain AUMW

Exposure of green microalgae to HMs, including Pb^{+2}, has been reported to cause a severe decline in their photosynthetic activity. Pb^{+2} disrupts the normal function of the photosynthetic machinery, for example, by replacing manganese (Mn) in Photosystem II. Also, Pb^{2+} is well-documented for reducing the production of enzymes involved in the synthesis of chlorophyll, as well as several enzymes that play a vital role in the Calvin cycle, resulting in a decrease in F_v/F_m [44]. A green microalgae *Scenedesmus acutus* has shown a significant decline in its F_v/F_m, with no effect on the electron transport rate of Photosystem II [45]. Additionally, Pb^{+2} imposes destructive effects on thylakoid membranes, causing membrane de-staking and peroxidation of membrane lipids, leading to the formation of reactive oxygen species. This results in oxidative damage to proteins and other macromolecules and inhibits the synthesis of enzymes that have functions in the Calvin cycle [46].

Considering the multi-level deleterious effects of Pb+2, it is important to determine the performance of photosystem II under Pb^{+2} stress conditions. The in-situ detection and quantification of stress-related markers of photosystem-II, such as NPQ and F_v/F_m, provide insights into the strain AUMW's stress response to Pb^{+2} exposure (Fig. 4). Notably, a sequential decrease in F_v/F_m and a rise in NPQ levels enabled the strain AUMW to withstand Pb^{+2} concentrations of 100 and 200 ppm. The initial response involved an obvious reduction in F_v/F_m within the first 6 h of incubation, with the maximum decline observed in sample X1. An initial drop and subsequent increase in NPQ levels during this period were concurrently observed, indicating the addition of Pb^{+2} promoted photosynthetic activity of strain AUMW's in treatments X2 and X3 compared to control X1. These stress-related trends were consistent with OD_{750} (Fig. 3b), and cell proliferation data (Fig. 3c and d).

Over time, the algae strain AUMW demonstrated resilience to Pb^{+2} stress. From 24 to 72 h of exposure, a concentration-dependent alteration in stress response was evident—there was a notable decrease in F_v/F_m at 24 h followed by its recovery, and a significant peak of NPQ at 48 h, followed by a decrease at 72 h post-incubation. The maximal stress response by strain AUMW was observed in X3 at 200 ppm of Pb^{+2}, while X2 at 100 ppm demonstrated no obvious signs of Pb^{+2} stress, as inferred from the rising F_v/F_m and falling NPQ levels compared to X1. In summary, strain AUMW adapted to Pb^{+2} stress by dynamically modulating F_v/F_m and NPQ levels, indicative of a sophisticated stress mitigation mechanism. Our findings not only revealed the temporal dynamics of stress impact but also highlighted the resilience of photosynthetic machinery in the face of Pb^{+2} exposure, enriching our understanding of algal adaptive capacity.

3.5. Mechanistic insights into Pb^{+2} removal

3.5.1. Cell surface adsorption phenomena

The PAM fluorometry analysis illuminated critical insights into the Pb^{+2} removal dynamics of strain AUMW at intervals of 1, 24, and 72 h following exposure to 100 ppm (X2) and 200 ppm (X3) concentrations. These intervals were key for delineating the temporal aspects of the mechanisms involved in the removal of Pb^{+2}. Field Emission Scanning Transmission Electron Microscopy (FE-STEM) micrographs in both dark and bright field modes revealed the biomineralization of Pb^{+2} on the cellular surface as the predominant removal strategy at these time points (Fig. 5). Elemental mapping (EM) confirmed on surface distribution of mineralized lead (Pb) (indicated by saiyan blue), also, pinpointed the cellular distribution of key elements: C (purple), O (red), and Si (green), which are vital for algal structural integrity, adaptation to abiotic stresses, and metabolic processes [47,48]. Interestingly, Si's function in green microalgae, despite its significance for diatom growth, DNA replication, and chlorophyll synthesis [49], remains obscure. Thus, the micrographs depicted element C as the dominant constituent of the algal cell (Fig. 5a3 – f3), exhibiting an amorphous configuration via electron diffraction patterns (Fig. 5a8 – f8). The presence of Pb, O, and Si elements was concurrently detected on the surface of algae from X2 and X3 (Fig. 5a4, a5, a6 – f4, f5, f6) at each selected time interval. Stacked images highlighted element C amidst Pb (Fig. 5a4′-f4′), O (Fig. 5a5′-f5′), and Si (Fig. 5a6′-f6′) signatures, suggesting their roles in encapsulating the carbon-rich algal cell

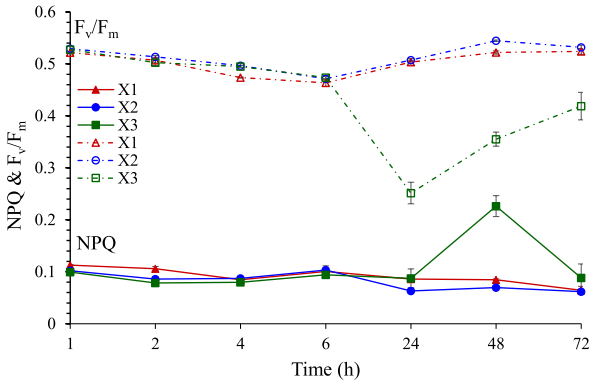

Fig. 4. *In situ* elucidation of strain AUMW's resilience mechanisms to Pb+2 stress. This figure depicts the adaptive mechanisms of strain AUMW to withstand stress induced by Pb+2, as deduced from measurements of quantum yield (*Fv/Fm*) and non-photochemical quenching (NPQ) across different time points.

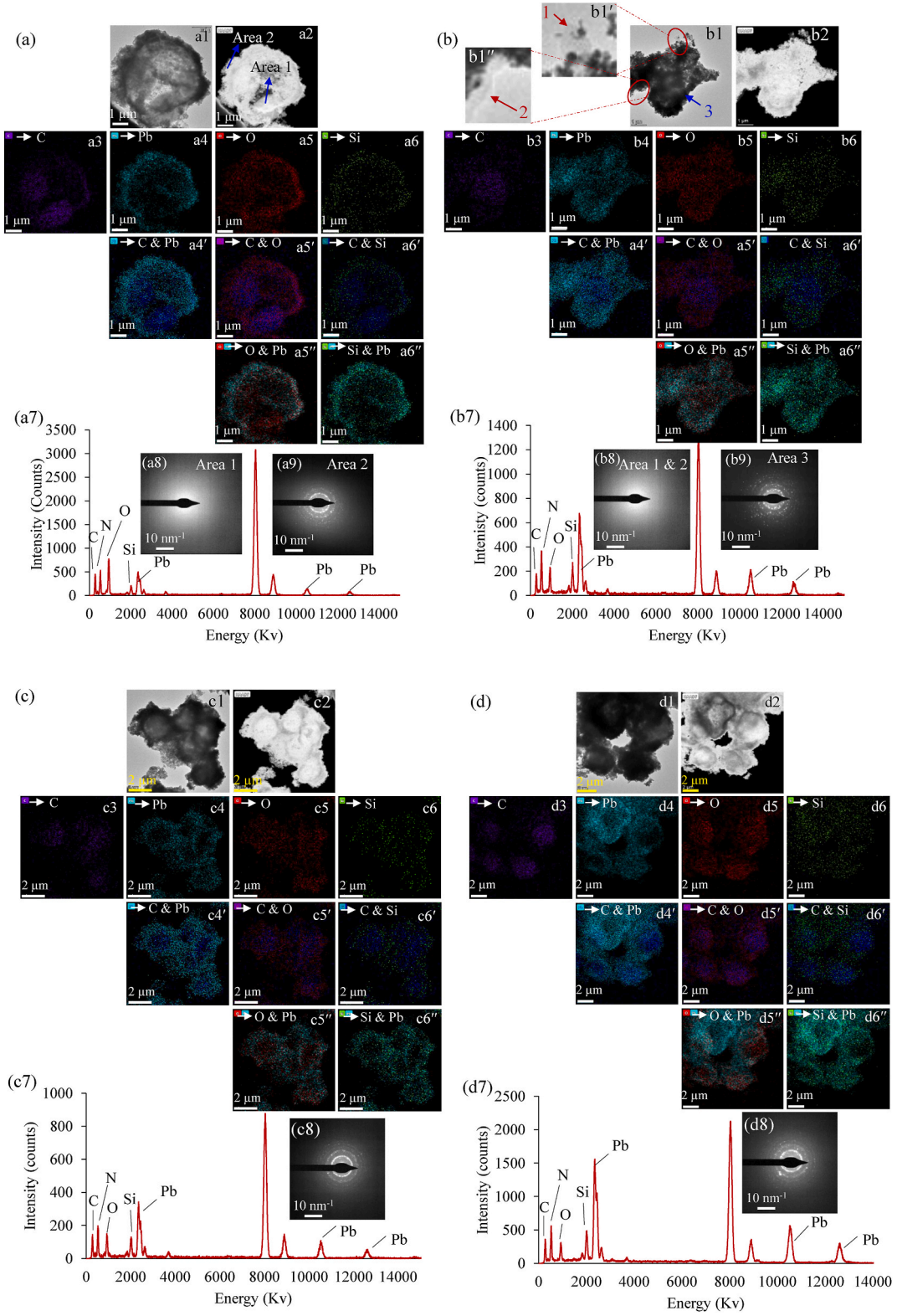

Fig. 5. Mechanisms of Pb+2 removal by strain AUMW in F/2 medium with Pb+2 supplementation. Characterization of material interactions and deposition on the cellular surface through transmission electron microscopy (TEM), elemental mapping (EM), energy-dispersive X-ray spectroscopy (EDS), and electron diffraction at varying time intervals. Each panel displays the medium supplemented with different concentrations of Pb+2 after

specific exposure times: **(a)** 100 ppm Pb+2 after 1 h, **(b)** 200 ppm Pb+2 after 1 h, **(c)** 100 ppm Pb+2 after 24 h, **(d)** 200 ppm Pb+2 after 24 h, **(e)** 100 ppm Pb+2 after 72 h, and **(f)** 200 ppm Pb+2 after 72 h.

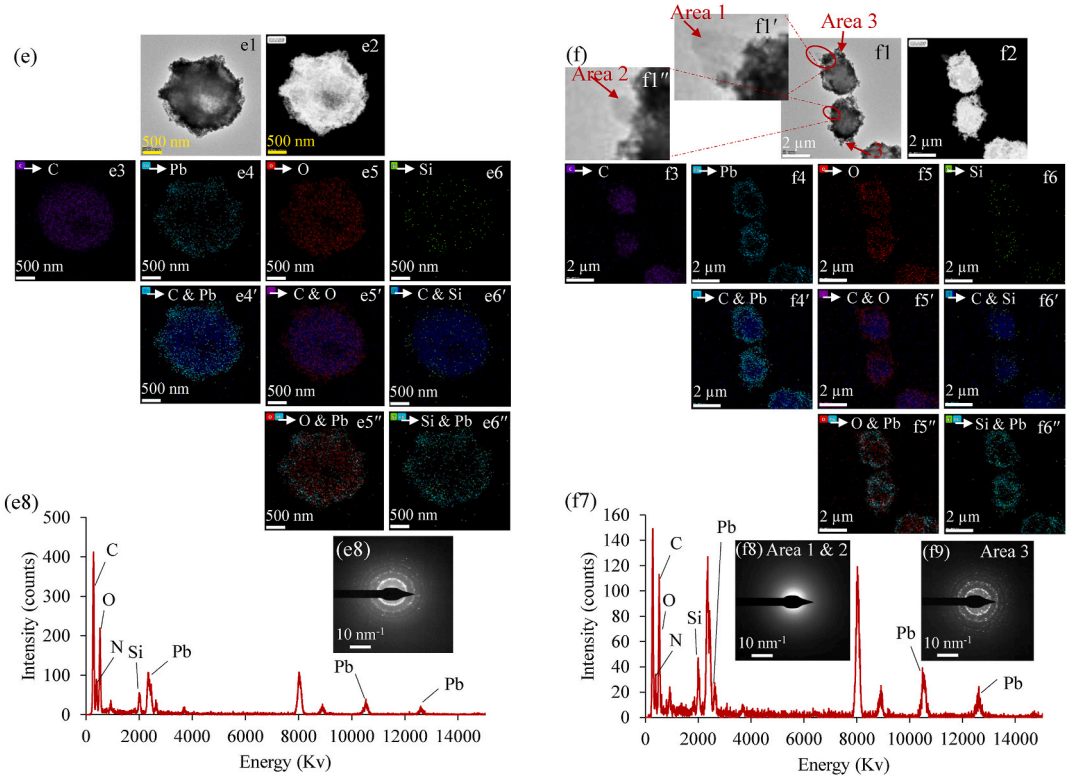

Fig. 5. (*continued*).

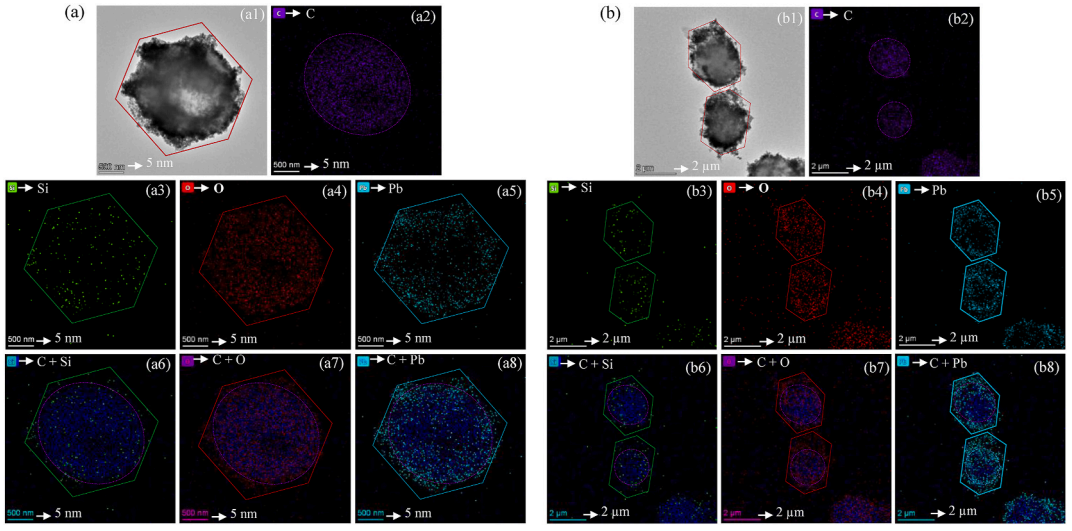

Fig. 6. Elemental mapping reveals surface silicification and enhanced algal resilience to Pb+2 exposure. Data were collected 72 h post-exposure to **(a)** 100 ppm and **(b)** 200 ppm of Pb+2. **(a1, b1)** Bright-field micrographs highlight the algal cell morphology with red-lined hexagons indicating silicification on the surface. Color indicators for elements within the hexagon are purple for carbon (C), green for silicon (Si), blue for oxygen (O), and saiyan blue for lead (Pb). **(a2, b2)** Carbon signatures are delineated by purple-dotted ovals surrounding the algal cells. Sequential images **(a3–a5, b3–b5)** display the individual signatures of Si, O, and Pb. Composite images **(a6–a8, b6–b8)** show the overlay of C, Si, O, and Pb signatures, illustrating the adsorption on the strain AUMW's cell surfaces, manifesting a transformation from the natural oval shape of the cells to hexagonal appearances.

(Fig. 5a4′-f4′, a5′-f5′, a6′-f6′).

These findings proposed that element oxygen could be a part of various macromolecules of the strain AUMW's cell wall, playing a vital role in scavenging Pb^{+2} and traces of Si present in the cultivation medium. Furthermore, the overlapped micrographs of elements O (Fig. 5a5″-f5″) and Si (Fig. 5a6″-f6″) featuring Pb revealed a consistent distribution of element O in the center, while partially hollow zones were evident in the latter case. This suggests that Si and Pb^{+2} were externally mineralized on the algal surface. Furthermore, the presence of Pb, O, and Si on the surface of strain AUMW was confirmed by energy dispersion spectroscopy (EDS) (Fig. 5a7-f7). Additionally, electron diffraction patterns obtained from specified locations on the surface of the algal cells verified that bio-mineralized Pb was crystalline (Fig. 5A9, b9, c8, d9, e8 & f9), while Si (Fig. 5a8, b8, & f8) appeared amorphous. Similar results confirmed a significant enhancement in the biomineralization of Pb^{+2} on the surface of algae harvested from treatment X3 when compared with algae obtained from treatment X2 (Fig. 5b–d, and f).

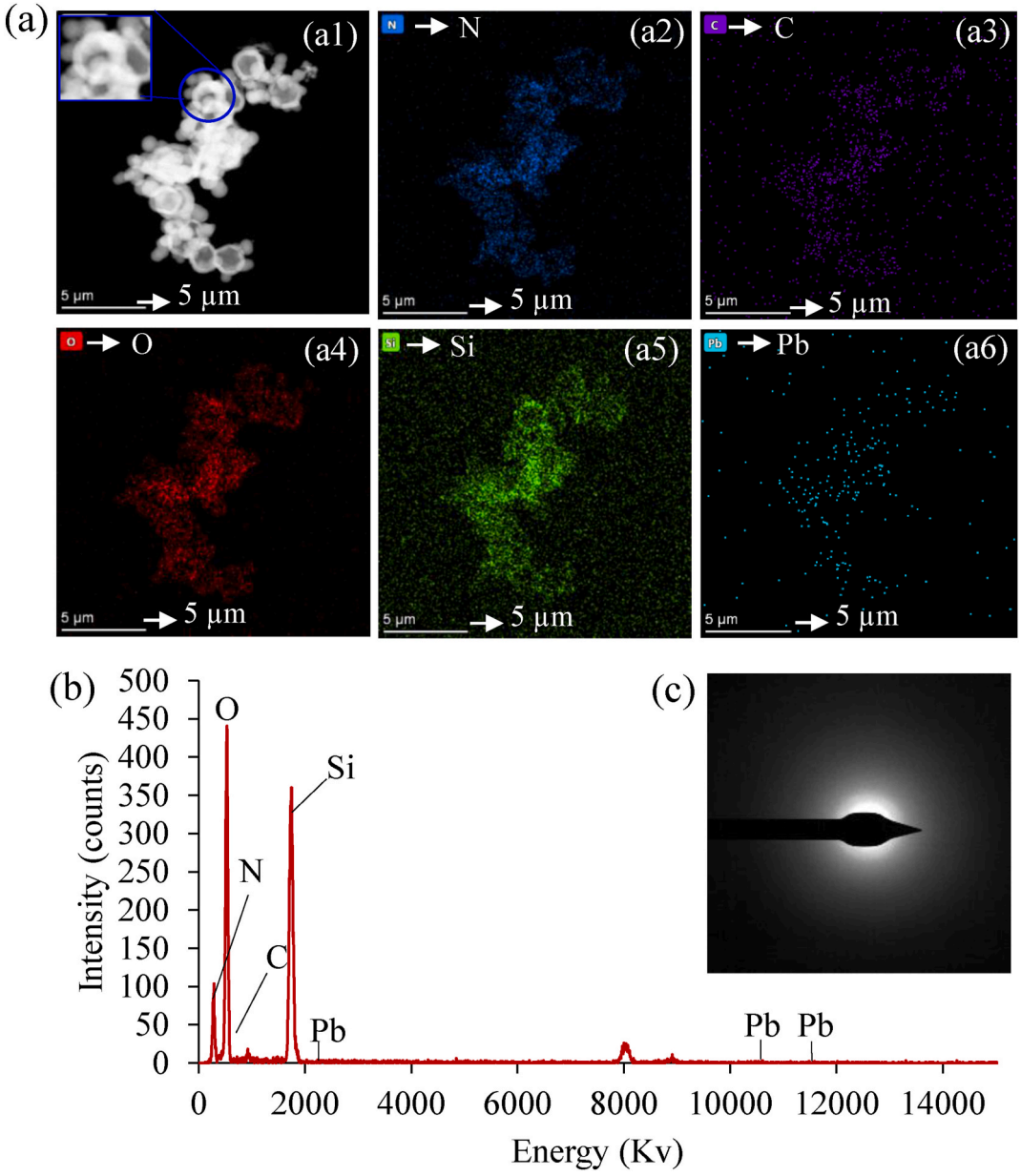

Fig. 7. Characterization of silicification in silica hexagons. **(a)** Transmission electron microscopy (TEM) and elemental mapping analysis of the silicified structure. **(a1)** A dark-field TEM image revealing the fine details of the silicified silica. **(a2-a6)** Elemental maps indicating the distribution of specific elements within the structure, color-coded as follows: nitrogen (N) in blue, carbon (C) in purple, oxygen (O) in red, silicon (Si) in green, and lead (Pb) in saiyan blue. **(b)** Energy-dispersive X-ray spectroscopy (EDS) spectrum validating the elemental composition and relative abundance. **(c)** Selected area electron diffraction pattern illustrating the amorphous nature of the silicified material.

3.5.2. Silica as a defensive barrier emergent extracellular silicification enhanced strain AUMW resilience to Pb^{+2}

Our research provides evidence of extracellular silicification playing a pivotal role in the cellular structural integrity and stress resistance of the green microalgae that is strain AUMW against Pb^{+2} (Fig. 6). The strain AUMW cells sampled from treatments X2 (Fig. 6a) and X3 (Fig. 6b), served as templates for silica biomineralization, forming hexagonal, shell-like geometric structures on the algal surfaces.

The Bright-Field Transmission Electron Microscopy (BF-TEM) images obtained from the microalgal cells at 72 h after exposure to 100 ppm and 200 ppm of $Pb(N_2O_6)$ in the X2 and X3 treatments, respectively (Fig. 6a1 & b1), exhibit clear indications of lead mineralization giving distinct hexagonal morphology to the cells, which are demarcated by solid red lines. This hexagonal structuring underscores the microalgal adaptation to elevated Pb^{+2} levels, shedding light on the cellular assimilation and biomineralization pathways precipitated by lead accumulation. Further scrutiny, focusing on carbon— the paramount constituent of microalgal cellular structure—via carbon mapping analysis, has unveiled an ovate cellular morphology, highlighted with a purple dotted line (Fig. 6a2 & b2). The uniform distribution of carbon across the cell suggests that the microalgae preserve structural integrity, with no apparent deterioration of the cell wall. This morphological resilience highlights cell robustness and enhances understanding of lead dynamics within microalgal systems.

Further analysis identified an uncharacterized component shaping the microalgae, confirmed by EM-analysis as Si (green) (Fig. 6a3 & b3). Elemental Si typically exists as silicic acid, requiring oxygen; thus, elemental O (red) localization correlates with microalgal hexagonal cellular morphology (Fig. 6a4 & b4). This is supported by Pb mineralization matching hexagonal shapes, outlined in cyan-blue and highlighted with solid saiyan-blue hexagonal lines (Fig. 6a5 & b5). Overlapped views of C with Si (Fig. 6a6 & b6), C with O elements (Fig. 6a7 & b7), and C with Pb element (Fig. 6a8 & b8) further support interactions and mineralization of these elements on algal surface. The results unambiguously demonstrate that microalgal cells serve as a scaffold for the Si element, which, in synergism with O, polymerizes to form a hexagonal sheath encapsulating the microalgal cells. This encapsulation notably safeguards the algal cells from the cytotoxic effects of Pb^{+2}, while simultaneously enhancing the sequestration of Pb^{+2}. The enhanced immobilization of Pb^{+2} is indicative of a potentially effective biological mechanism for mitigating heavy metal contamination in affected environments.

The self-polymerization of silicon observed in our samples was distinctly captured in dark field TEM micrographs (Fig. 7a1), verified by EM analysis (Fig. 7a5). EM identified a pronounced presence of nitrogen (N), indicated by a blue colour (Fig. 7a2), and C (purple) (Fig. 7a3), respectively. The presence of these elements suggests the occurrence of specific biomolecules, suggesting that algal cells might be encapsulated by silica hexagonal shells but after cell wall denaturation/death the algal cells left the hexagon shell-like structures. An increased presence of O (red), as shown in Fig. 7a4, seems to promote the mineralization process of Pb^{+2} (saiyan blue) (Fig. 7a6). The EDS spectrum (Fig. 7b) demonstrates a significantly higher intensity of Si and O elements. This implies that the predominant form of Si is silicic acid, a form extensively distributed within the Earth's crust [50]. The electron diffraction pattern (Fig. 7c), derived from the blue-circled analytical points in Fig. 7a1, confirms that the polymerized silicon structure is amorphous in nature. To our knowledge, this study is the first to report of an extracellular silicification on the surface of green microalgae, proposing a novel role for this mechanism in increasing the algal resistance to Pb^{+2}.

3.6. Determining the source of silicon by FTIR

The source of Si was identified by elucidation of the chemical composition of major ingredients of algal cultivation medium via FTIR analysis (Fig. S2a), while the intensity of Si was quantified by EM-analysis (Fig. S2b). The peaks at 1242-1384 cm^{-1} exhibit the presence of amide II [51], $(CO_3)^{2-}$ [52] and Si–OH bonds, while peak at 1020 cm^{-1} and 1040-1045 cm^{-1} represents the occurrence of Si–O–Si/Si–O–Pb and C–O(H) stretching vibration of ethylene glycol [53]. While the peak at 608 cm^{-1} corresponds to Si–Si stretching vibration [54].

3.7. Plausible explanation of the silicification process

Please refer to section 1 in the supplementary manuscript file.

3.8. Conclusion

In this work, we conducted a comprehensive analysis of the green microalgae *Micractinium belenophorum* strain AUMW, newly isolated from a lead mining site. Our findings highlight its remarkable tolerance to Pb^{+2} levels (20 ppm–200 ppm) and novel survival mechanisms for lead removal. Key results include: i) Strain AUMW shows high tolerance to Pb^{+2} levels up to 200 ppm; ii) Using RSM, we optimized conditions, achieving 99.6 % Pb^{+2} removal; iii) Strain AUMW modulates Photosystem II (F_v/F_m and NPQ) to mitigate Pb^{+2} toxicity; iv) Pb^{+2} exposure enhanced photosynthetic activity and growth (OD_{750}, cell number, and cell size); v) Strain AUMW utilizes extracellular silicification to create a physical barrier, reducing intracellular Pb^{+2} accumulation and enhancing removal via surface sequestration. These results support our hypothesis that strain AUMW evolved unique mechanisms to thrive in lead-rich environments, enabling it to eliminate Pb^{2+} toxicity at levels far exceeding environmental permissible limits. This study suggests potential applications for strain AUMW in bioremediation and heavy metal recycling from polluted sites, spent batteries, and in biotechnological engineering for high tolerance/sequestration traits in plants and microalgae. Further research is needed to elucidate the genetic and molecular mechanisms underlying the extracellular silicification process.

Data availability statement

The data are included in article and supplementary materials in this article.

CRediT authorship contribution statement

Fiaz Ahmad: Writing – review & editing, Writing – original draft, Validation, Resources, Project administration, Methodology, Investigation, Funding acquisition, Data curation, Conceptualization. **Michael Manefield:** Writing – review & editing, Validation, Methodology.

Declaration of competing interest

The authors declare that they have no known competing financial interests or personal relationships that could have appeared to influence the work reported in this paper.

Acknowledgements

This research was financially supported by the research startup funds provided by Northwestern Polytechnical University (NPU), Xi'an, China (23GH02022), and National Natural Science Foundation of China (NSFC), Research Funds for International Young Scientists (RFIS-I) (32350410426).

Appendix A. Supplementary data

Supplementary data to this article can be found online at https://doi.org/10.1016/j.heliyon.2024.e36366.

References

[1] D. Pal, S.K. Maiti, Evaluation of potential human health risks from toxic metals via consumption of cultured fish species *Labeo rohita*: a case study from an urban aquaculture pond, Exposure Health 11 (2019) 33–46, https://doi.org/10.1007/s12403-017-0264-8.
[2] S.S. Habib, S. Naz, M.Q. Saeed, J.A. Ujan, S. Masud, A. Mushtaq, M. Ullah, K. Khan, M. Zahid, S.S. Al-Rejaie, M. Mohany, Assessment of heavy metal levels in polyculture fish farms and their aquatic ecosystems: an integrative study addressing environmental and human health risks associated with dam water usage, Environ. Geochem. Health 46 (2024) 267, https://doi.org/10.1007/s10653-024-02042-y.
[3] B. Larsen, E. Sanchez-Triana, Global health burden and cost of lead exposure in children and adults: a health impact and economic modelling analysis, Lancet Planet, Heat 7 (2023) e831–e840, https://doi.org/10.1016/S2542-5196(23)00166-3.
[4] Q. Liang, K. Tian, L. Li, Y. He, T. Zhao, B. Liu, Q. Wu, B. Huang, L. Zhao, Y. Teng, Ecological and human health risk assessment of heavy metals based on their source apportionment in cropland soils around an e-waste dismantling site, Southeast China, Ecotoxicol. Environ. Saf. 242 (2022) 113929, https://doi.org/10.1016/j.ecoenv.2022.113929.
[5] Y. Pan, M. Chen, X. Wang, Y. Chen, Ecological risk, source apportionment, and influencing factors of heavy metals in soil in a typical lead-zinc mining watershed, Guangxi, China, J. Environ. Chem. Eng. 12 (2024) 112731.
[6] Z. Ranjbar, D. Pourhadadi, S. Montazeri, M. Roshanzamir Modaberi, Lead compounds in paint and coatings: a review of regulations and latest updates, Prog. Org. Coating 174 (2023) 107247, https://doi.org/10.1016/j.jece.2024.112731.
[7] X. Zhou, W. Liu, J. Zhang, C. Wu, X. Ou, C. Tian, Z. Lin, Z. Dang, Biogenic calcium carbonate with hierarchical organic–inorganic composite structure enhancing the removal of Pb(II) from wastewater, ACS Appl. Mater. Interfaces 9 (2017) 35785–35793, https://doi.org/10.1021/acsami.7b09304.
[8] C. Aibeche, N. Selami, F.E.-H. Zitouni-Haouar, K. Oeunzar, A. Addou, M. Kaid-Harche, A. Djabeur, Bioremediation potential and lead removal capacity of heavy metal-tolerant yeasts isolated from Dayet Oum Ghellaz Lake water (northwest of Algeria), Int. Microbiol. 25 (2022) 61–73, https://doi.org/10.1007/s10123-021-00191-z.
[9] R. Shahrokhi-Shahraki, C. Benally, M.G. El-Din, J. Park, High efficiency removal of heavy metals using tire-derived activated carbon vs commercial activated carbon: insights into the adsorption mechanisms, Chemosphere 264 (2021) 128455, https://doi.org/10.1016/j.chemosphere.2020.128455.
[10] X. Xiao, Y. Sun, J. Liu, H. Zheng, Flocculation of heavy metal by functionalized starch-based bioflocculants: characterization and process evaluation, Sep. Purif. Technol. 267 (2021) 118628, https://doi.org/10.1016/j.seppur.2021.118628.
[11] F. Almomani, R.R. Bhosale, Bio-sorption of toxic metals from industrial wastewater by algae strains *Spirulina platensis* and *Chlorella vulgaris*: application of isotherm, kinetic models and process optimization, Sci. Total Environ. 755 (2021) 142654, https://doi.org/10.1016/j.scitotenv.2020.142654.
[12] P. Bokade, H.J. Purohit, A. Bajaj, Myco-remediation of chlorinated pesticides: insights into fungal metabolic system, Indian J. Microbiol. 61 (2021) 237–249, https://doi.org/10.1007/s12088-021-00940-8.
[13] A. Soudani, A. Gholami, M. Mohammadi Roozbahani, S. Sabzalipour, A. Mojiri, Heavy metal phytoremediation of aqueous solution by *Typha domingensis*, Aquat. Ecol. 56 (2022) 513–523, https://doi.org/10.1007/s10452-022-09945-x.
[14] X. Cheng, L. Sheng, S. Peng, E. Thorley, H. Cao, K. Li, Integrated mechanism of heavy metal bioremediation from soil to rice (*Oryza sativa* L.) mediated by *Enterococcus faecium*, Plant Growth Regul. 97 (2022) 523–535, https://doi.org/10.1007/s10725-022-00811-2.
[15] K. Yin, Q. Wang, M. Lv, L. Chen, Microorganism remediation strategies towards heavy metals, Chem. Eng. J. 360 (2019) 1553–1563, https://doi.org/10.1016/j.cej.2018.10.226.
[16] F. Ahmad, N. Ashraf, R.-B. Zhou, J.J. Chen, Y.-L. Liu, X. Zeng, F.-Z. Zhao, D.-C. Yin, Optimization for silver remediation from aqueous solution by novel bacterial isolates using response surface methodology: recovery and characterization of biogenic AgNPs, J. Hazard Mater. 380 (2019) 120906, https://doi.org/10.1016/j.cej.2018.10.226.
[17] F. Khanramaki, A.R. Keshtkar, Optimization of thorium solvent extraction process from feed solution with Cyanex 272 by response surface methodology (RSM), Sci. Rep. 14 (2024) 15131, https://doi.org/10.1038/s41598-024-66091-0.
[18] M. Mubashar, M. Naveed, A. Mustafa, S. Ashraf, K. Shehzad Baig, S. Alamri, M.H. Siddiqui, M. Zabochnicka-Swiatek, M. Szota, H.M. Kalaji, Experimental investigation of *Chlorella vulgaris* and *Enterobacter* sp. MN17 for decolorization and removal of heavy metals from textile wastewater, Water 12 (2020) 3034, https://doi.org/10.3390/w12113034.

[19] O. Nateras-Ramirez, M.R. Martínez-Macias, D.I. Sanchez-Machado, J. Lopez-Cervantes, R.J. Aguilar-Ruiz, An overview of microalgae for Cd^{2+} and Pb^{2+} biosorption from wastewater, Bioresour. Technol. Rep. 17 (2022) 100932, https://doi.org/10.1016/j.biteb.2021.100932.

[20] N.A. Politaeva, Y.A. Smyatskaya, E.A. Tatarintseva, Using adsorption material based on the residual biomass of *Chlorella Sorokiniana* microalgae for wastewater purification to remove heavy metal ions, Chem. Petrol. Eng. 55 (2020) 907–912, https://doi.org/10.1007/s10556-020-00712-z.

[21] N. Ashraf, F. Ahmad, Y. Lu, Synergy between microalgae and microbiome in polluted waters, Trends Microbiol. 31 (2023) 9–21, https://doi.org/10.1016/j.tim.2022.06.004.

[22] P.S. Chandrashekharaiah, Y. Gupte, P. Sarkar, S. Prasad, D. Sanyal, S. Dasgupta, A. Banik, Algae-bacterial aquaculture can enhance heavy metals (Pb^{2+} and Cd^{2+}) remediation and water re-use efficiency of synthetic streams, Resour. Conserv. Recycl. 180 (2022) 106211, https://doi.org/10.1016/j.resconrec.2022.106211.

[23] F. Ahmad, S. Anwar, S. Firdous, Y. Da-Chuan, S. Iqbal, Biodegradation of bispyribac sodium by a novel bacterial consortium BDAM: optimization of degradation conditions using response surface methodology, J. Hazard Mater. 349 (2018) 272–281, https://doi.org/10.1016/j.jhazmat.2017.12.065.

[24] G. Kaur, N. Singh, A. Rajor, RSM-CCD optimized *Prosopis juliflora* activated carbon for the adsorptive uptake of ofloxacin and disposal studies, Environ. Technol. Innovat. 25 (2022) 102176, https://doi.org/10.1016/j.eti.2021.102176.

[25] E.S. Krivina, A.D. Temraleeva, Y.S. Bukin, Species delimitation and microalgal cryptic diversity analysis of the genus *Micractinium* (Chlorophyta), Vavilov J. Genet. Breed. 26 (2022) 74–85, 10.18699/VJGB-22-11.

[26] H. Padmi, V.D. Kharisma, A.N.M. Ansori, M.T. Sibero, M.H. Widyananda, E. Ullah, O. Gumenyuk, S. Chylichcova, N. Bratishko, E.S. Prasedya, Macroalgae bioactive compounds for the potential antiviral of SARS-CoV-2: an in silico study, J. Pure Appl. Microbiol. 16 (2022) 1018–1027, https://doi.org/10.22207/JPAM.16.2.26.

[27] H. Padmi, A. Ansori, R. Probojati, A. Murtadlo, A. Sunarwidhi, A. Hernawan, H. Sunarpi, S. Widyastuti, A. Nikmatullah, E. Prasedya, Anti-inflammatory potential of λ-carrageenan by inhibition of IL-6 receptor: in silico study, in: IOP Conference Series: Earth and Environmental Science, IOP Publishing, 2021 012106, https://doi.org/10.1088/1755-1315/913/1/012106.

[28] Stelmach Pessi, N. Rybalka, T. Friedl, J. Boy, A. Wilmotte, Microalgae diversity along an Antarctic glacier forefield. Poster Session Presented at SCAR Biennial Meetings and Open Science Conference 2016, Kuala Lumpur, Malaysia, August 2016. https://hdl.handle.net/2268/206812.

[29] W. Liu, D. Fu, T. Pan, R.P. Singh, Characterization and polyculture analysis of microalgae strains based on biomass production and nutrient consumption, and bacterial community in municipal wastewater, Water 13 (2021) 3190, https://doi.org/10.3390/w13223190.

[30] A.T. Couto, M. Cardador, S. Santorio, L. Arregui, B. Sicuro, A. Mosquera-Corral, P.M.L. Castro, C.L. Amorim, Cultivable microalgae diversity from a freshwater aquaculture filtering system and its potential for polishing aquaculture-derived water streams, J. Appl. Microbiol. 132 (2022) 1543–1556, https://doi.org/10.1111/jam.15300.

[31] N. Ashraf, F. Ahmad, C. Jing Jie, Z. Tuo Di, Z. Feng-Zhu, D.-C. Yin, Optimization of *Enterobacter cloacae* mediated synthesis of extracellular silver nanoparticles by response surface methodology and their characterization, Part. Sci. Technol. 38 (2020) 931–943, https://doi.org/10.1080/02726351.2019.1636915.

[32] M.M. Rahman, N. Hosano, H. Hosano, Recovering microalgal bioresources: a review of cell disruption methods and extraction technologies, Molecules 27 (2022) 2786, https://doi.org/10.3390/molecules27092786.

[33] N. Ashraf, F. Ahmad, Y. Lu, D.-C. Yin, Bacterial extracellular protein interacts with silver ions to produce protein-encapsulated bactericidal AgNPs, Process Biochem. 106 (2021) 120–129, https://doi.org/10.1016/j.procbio.2021.04.006.

[34] S.K. T, M.N.D. Bs, L.R. Babu, A.E. Paul, S. Murugan, R. Periakaruppan, Nanozymes as catalytic marvels for biomedical and environmental concerns: a chemical engineering approach, J. Cluster Sci. 35 (2024) 715–740, https://doi.org/10.1007/s10876-023-02524-6.

[35] X. Xiao, W. Li, M. Jin, L. Zhang, L. Qin, W. Geng, Responses and tolerance mechanisms of microalgae to heavy metal stress: a review, Mar. Environ. Res. 183 (2023) 105805, https://doi.org/10.1016/j.marenvres.2022.105805.

[36] Y. Ding, R. He, C. Wang, Q. Wei, X. Ma, G. Yang, Efficient separation of Cd^{2+} and Pb^{2+} by *Tetradesmus obliquus*: insights from cultivation conditions with competitive adsorption modeling, J. Water Process Eng. 60 (2024) 105207, https://doi.org/10.1016/j.jwpe.2024.105207.

[37] M. Kumar, A.K. Singh, M. Sikandar, Study of sorption and desorption of Cd (II) from aqueous solution using isolated green algae Chlorella vulgaris, Appl. Water Sci. 8 (2018) 225, https://doi.org/10.1007/s13201-018-0871-y.

[38] M. Plohn, C. Escudero-Onate, C. Funk, Biosorption of Cd(II) by Nordic microalgae: tolerance, kinetics and equilibrium studies, Algal Res. 59 (2021) 102471, https://doi.org/10.1016/j.algal.2021.102471.

[39] S. Gu, C.Q. Lan, Effects of culture pH on cell surface properties and biosorption of Pb(II), Cd(II), Zn(II) of green alga *Neochloris oleoabundans*, Chem. Eng. J. 468 (2023) 143579, https://doi.org/10.1016/j.cej.2023.143579.

[40] X. Liu, H. Yin, H. Liu, Y. Cai, X. Qi, Z. Dang, Multicomponent adsorption of heavy metals onto biogenic hydroxyapatite: surface functional groups and inorganic mineral facilitating stable adsorption of Pb(II), J. Hazard Mater. 443 (2023) 130167, https://doi.org/10.1016/j.jhazmat.2022.130167.

[41] Y. Lin, J. Abraham, A. RoyChowdhury, T.-L. Su, W. Braida, C. Christodoulatos, Ecotoxicological response of Scenedesmus obliquus to pure energetic compounds and metal ions found in wastewater streams from munitions manufacturing, Algal Res. 48 (2020) 101927, https://doi.org/10.1016/j.algal.2020.101927.

[42] S. Abinandan, S.R. Subashchandrabose, L. Panneerselvan, K. Venkateswarlu, M. Megharaj, Potential of acid-tolerant microalgae, *Desmodesmus* sp. MAS1 and *Heterochlorella* sp. MAS3, in heavy metal removal and biodiesel production at acidic pH, Bioresour. Technol. 278 (2019) 9–16, https://doi.org/10.1016/j.biortech.2019.01.053.

[43] T. Amjadi, J. Razeghi, R. Motafakkerazad, R. Zareipour, Interaction between *Haematococcus pluvialis* microalgae and lead nitrate: lead adsorption from water, Int. J. Phytoremediation 26 (2024) 1168–1179, https://doi.org/10.1080/15226514.2023.2298773.

[44] B. Nowicka, Heavy metal–induced stress in eukaryotic algae—mechanisms of heavy metal toxicity and tolerance with particular emphasis on oxidative stress in exposed cells and the role of antioxidant response, Environ. Sci. Pollut. Res. 29 (2022) 16860–16911, https://doi.org/10.1007/s11356-021-18419-w.

[45] L.-L. Dong, H.-X. Wang, Y. Wang, X.-Q. Hu, X.-L. Wen, Effects of Cd^{2+} and Pb^{2+} on growth and photosynthesis of two freshwater algae species, Pol. J. Environ. Stud. 31 (2022) 2059–2068, https://doi.org/10.15244/pjoes/143256.

[46] F. Marchetto, S. Santaeufemia, M. Lebiedzinska-Arciszewska, M.A. Sliwińska, M. Pich, E. Kurek, A. Nazieblo, M. Strawski, D. Solymosi, M. Szklarczyk, E. Bulska, J. Szymanski, M. Wierzbicka, Y. Allahverdiyeva, M.R. Wieckowski, J. Kargul, Dynamic adaptation of the extremophilic red microalga *Cyanidioschyzon merolae* to high nickel stress, Plant Physiol. Biochem. 207 (2024) 108365, https://doi.org/10.1016/j.plaphy.2024.108365.

[47] Z.V. Finkel, M.J. Follows, J.D. Liefer, C.M. Brown, I. Benner, A.J. Irwin, Phylogenetic diversity in the macromolecular composition of microalgae, PLoS One 11 (2016) e0155977, https://doi.org/10.1371/journal.pone.0155977.

[48] Y. Zhang, X. Kang, F. Zhen, Z. Wang, X. Kong, Y. Sun, Assessment of enzyme addition strategies on the enhancement of lipid yield from microalgae, Biochem. Eng. J. 177 (2022) 108198, https://doi.org/10.1016/j.bej.2021.108198.

[49] C. Exley, A. Tollervey, G. Gray, S. Roberts, J.D. Birchall, Silicon, aluminium and the biological availability of phosphorus in algae, Proc. R. Soc. Lond. Ser. B Biol. Sci. 253 (1993) 93–99, https://doi.org/10.1098/rspb.1993.0086.

[50] Q. Song, Q. He, J. Nie, T. Song, H. Zhou, Y. Hu, Y. Chen, Y. Deng, F. Cheng, The properties of magnesium silicate hydrate prepared from the magnesium silicate minerals in the earth's crust, Buildings 14 (2024) 1188, https://doi.org/10.3390/buildings14051188.

[51] P. Rai, V. Singh, J. Sharma, S. Sharma, N. Sharma, M. Sharma, Application of WDXRF and FT-IR for Human Tooth Analysis, vol. 34, 2019, pp. 23–31.

[52] O. Saisa-ard, W. Somphon, W. Dungkaew, K.J. Haller, Evidence of a lead metathesis product from calcium hydroxyapatite dissolution in lead nitrate solution, Adv. Mater. Sci. Eng. 2014 (2014) 273632, https://doi.org/10.1155/2014/273632.

[53] Y. Qiu, S. Yang, H. Deng, L. Jin, W. Li, A novel nanostructured spinel $ZnCo_2O_4$ electrode material: morphology conserved transformation from a hexagonal shaped nanodisk precursor and application in lithium ion batteries, J. Mater. Chem. 20 (2010) 4439–4444, https://doi.org/10.1039/C0JM00101E.

[54] S. Kalem, P. Werner, V. Talalaev, M. Becker, O. Arthursson, N. Zakharov, Photoluminescence from silicon nanoparticles embedded in ammonium silicon hexafluoride, Nanotechnology 21 (2010) 435701, https://doi.org/10.1088/0957-4484/21/43/435701.